Sea-ice melt determines seasonal phytoplankton dynamics and delimits the habitat of temperate Atlantic taxa as the Arctic Ocean atlantifies

Ellen Oldenburg[1] □, Ovidiu Popa[1], Matthias Wietz[2,3], Wilken-Jon von Appen[2], Sinhue Torres-Valdes[2], Christina Bienhold[2,3], Oliver Ebenhöh[1], Katja Metfies[2]

[1]Institute of Quantitative and Theoretical Biology, Heinrich-Heine-University Düsseldorf, Universitätsstr. 1, D-40225 Düsseldorf, Germany. □email: ellen.oldenburg@hhu.de
[2]Alfred Wegener Institute Helmholtz Centre for Polar and Marine Research, Bremerhaven, Am Handelshafen 12, D-27570 Bremerhaven, Germany.
[3]Max Planck Institute for Marine Microbiology, Celsiusstraße 1 D-28359 Bremen, Germany.

COMPETING INTERESTS

The authors declare no competing interests.

Abstract

The Arctic Ocean is one of the regions where anthropogenic environmental change is progressing most rapidly and drastically. The impact of rising temperatures and decreasing sea ice on Arctic marine microbial communities is yet not well understood. Microbes form the basis of food webs in the Arctic Ocean, providing energy for larger organisms. Previous studies have shown that Atlantic taxa associated with low light are robust to more polar conditions. In this study, we compared to which extent sea ice melt influences light-associated phytoplankton dynamics and biodiversity over two years at two mooring locations in the Fram Strait. One mooring is deployed in pure Atlantic water, and the second in the intermittently ice-covered Marginal Ice Zone. Time-series analysis of amplicon sequence variants abundance over a two-year period, allowed us to identify communities of co-occurring taxa that exhibit similar patterns throughout the annual cycle. We then examined how alterations in environmental conditions affect the prevalence of species. During high abundance periods of diatoms, polar phytoplankton populations dominated, while temperate taxa were weakly represented. Generally, polar pelagic and ice-associated taxa (such as *Fragilariopsis cylindrus* or *Melosira arctica*) were more prevalent in Atlantic conditions whereas temperate taxa (such as *Odontella aurita* or *Proboscia alata)* have limited potential to persist in colder ice-impacted waters. In contrast to previous assumptions, we think that sea-ice melt acts as a barrier to the horizontal extent of temperate diatoms by preventing their succession at places strongly influenced by polar conditions such as the melting sea ice.

Introduction

The Arctic is affected by rapid and drastic environmental changes. For instance, air temperatures rise four times (1) as quickly in the region compared to other regions on Earth (2). Arctic sea ice is one of the fastest changing components of the Earth system (3). Over the past decades, the area of Arctic sea ice declined at a rate of about 1 million km^2 in area extent per decade (3, 4). There are indications for a 40%

decline in ice thickness due to thicker and older ice cover (5). The geographical extent of warmer and more saline Atlantic water is expected to expand northwards into the Central Arctic Ocean (CAO), which consequently will become warmer and saltier, further accelerating sea-ice decline (6). This process, called Atlantification of the Arctic Ocean (6), coincides with altered physical conditions. Ecosystems shift towards a more temperate state including the appearance and range expansion of subarctic specie (7, 8, 9, 10, 11, 12, 13). If the temperature increases and the loss of sea-ice continue at their current pace, the Arctic Ocean will likely be seasonally ice-free by 2050 (14). In such a scenario, sea-ice melt-related processes, such as melt-water stratification of the upper layer of the ocean, that is currently observed in the marginal ice zone (MIZ), might become more important over more prolonged periods throughout the seasonal cycle, and a larger geographic area, with ecological consequences for the Arctic Ocean. The MIZ is usually covered with 15-80% sea ice (15, 16, 17, 18, 19, 20, 21) and its distribution, thickness, and melt dynamics are key drivers of productivity (22), carbon export, biogeochemical cycling, and pelagic-benthic coupling. As a result of decreasing sea ice extent and the expected Atlantification, larger areas of the Arctic Ocean might become favorable for pelagic temperate phytoplankton. As a study site, Fram Strait allows us to investigate the combined effects of Atlantification and seasonal ice cover on Arctic marine ecosystems. Moorings with a suite of physical and biogeochemical sensors, as well as autonomous sampling systems for molecular biodiversity studies (Remote Access Sampler RAS), are positioned at two different locations in Atlantic Waters of Fram Strait at ~79°N: central Fram Strait (mooring cluster "HG-IV") and in the eastern Fram Strait (mooring cluster "F4") -see Figure 1. F4 is located in the flow path of the West Spitsbergen Current (WSC). HG-IV is located in the vicinity of the interface between the WSC and the East Greenland Current (EGC). The WSC carries relatively warm and salty Atlantic Water via Fram Strait northwards towards the CAO, while the EGC exports cold ice-covered and less saline Polar Water (PW) from the CAO through Fram Strait. In the vicinity of HG-IV, some of the Atlantic Water (AW) is mixed in an eddy-rich area (23) as part of a subduction process (24, 25) with the outflowing colder and fresher water of the EGC. This area is frequently characterized by major sea-ice melt events, as sea-ice coverage regularly extends (26)

into the WSC, which carries temperate species towards the CAO. Thus, ecosystem functionality in the vicinity of the MIZ in the WSC might serve as a model for future biodiversity and ecosystem functionality in a seasonally ice-free CAO impacted by Atlantification and thereby inform on the potential of temperate taxa to thrive in a seasonally ice-covered Atlantic-influenced Ocean (27, 28, 29, 30).

Over the past decades, the transport of sea ice in both volume and velocity towards Fram Strait increased in the area of the Transpolar Drift due to the thinning Arctic pack ice (31, 32, 33). This led to a significant south-eastward extension of the MIZ into Fram Strait during certain years of the past decade. In 2017 the MIZ extended into large parts of the WSC during summer, including the two moorings (33). Conversely, the 2018 ice export was reduced to less than 40% relative to that between 2000 and 2017.

The associated meltwater-induced stratification promoted a longer phytoplankton bloom with a relatively shallow extent and reduced export flux (34). The summer of 2018 had a mixed layer regime and a shorter, more intense bloom compared to other periods. During the spring of that year, there was also an increased carbon export to the deep sea (35). The particularly warm year of 2018 may reflect the conditions of the CAO in the future. The native biodiversity of the communities is a key determinant of whether and how a community or an individual organism can respond to changing abiotic conditions (36). We, therefore, expect that studying the microbial communities and, in particular, comparing the seasonal dynamics between the years 2017 and 2018 can greatly improve our knowledge about the resilience of pelagic and sympagic organisms and how microbial diversity and seasonality scale with the environmental variability. Molecular biodiversity research using ribosomal meta-barcoding has substantially improved our comprehension of marine microbial diversity and distribution patterns during the last 20 years. (37, 38). As part of the FRAM Infrastructure Program (Frontiers in Arctic Marine Monitoring) and the long-term ecological research site LTER HAUSGARTEN, activities in Fram Strait provide information on Arctic marine eukaryotic microbial biodiversity and biogeography based on annually recurring measurements (since 1999) recently expanded by year-round, continuous sampling since 2016. We hypothesize that biodiversity

97 and seasonal succession in the Fram Strait are strongly impacted by sea-ice melt and the extent of
98 stratification (39).
99 In this study, we exploit this wealth of data through a combination of statistical and bioinformatic
100 approaches. The continuous data collected over two years were decomposed using a Fourier
101 transformation into a series of sinusoidal functions. Each function represents a specific amplicon sequence
102 variant (ASV) dynamic over time. By clustering the ASVs based on their seasonal fluctuation patterns, it
103 became possible to analyze the impact of different water regimes that occurred in 2017 and 2018, as
104 reported in Appen et al. 2021 (34), on both species and community levels. We could elucidate the effects
105 of sea-ice melt on the seasonal dynamics of the associated eukaryotic microbial communities as key
106 drivers of phytoplankton bloom phenology. By assessing the contribution of polar and temperate
107 phytoplankton taxa to eukaryotic microbial communities in the WSC over the annual cycle, we infer the
108 potential of polar taxa to thrive in ice-free Atlantic water and temperate taxa to expand to areas impacted
109 by sea-ice melt.
110

111 # MATERIALS AND METHODS

112 ## Sampling

113 The samples analyzed in this study were collected using McLane Remote Access Samplers (RAS) deployed in
114 conjunction with other oceanographic sensors over three individual annual cycles from June 2016 - August
115 2019 on long-term moorings at stations HG-IV (79.0118N 4.1666E) and F4 (79.0118N 6.9648E) of the LTER
116 HAUSGARTEN and FRAM in the Fram Strait (40). This study covers the period from January 2017 to
117 December 2018, i.e., two calendar years. One RAS was deployed at a depth between 24-29 m at HG-IV and
118 another at 23-26m - at F4. The RAS samplers contained 48 sterile bags, each collecting water samples of 500
119 mL at programmed sampling events every two weeks. Samples were preserved by adding 700 µl of half-
120 saturated mercuric chloride (7.5% w/v) to the bags prior to sampling. A sample reflects the pool of up to

two samples collected one hour apart in two individual bags. Following the recovery of the RAS devices, water samples were filtered using Sterivex filter cartridges with a pore size of 0.22 µm (Millipore, USA). Filters were then stored at -20°C for later processing.

Mooring and satellite data

Temperature, salinity, and dissolved oxygen concentration were measured with a CTD-O_2 attached to the RAS frame. Physical oceanography sensors were manufacturer-calibrated and processed as described in (41). Raw and processed mooring data are available at PANGAEA https://doi.org/10.1594/PANGAEA.904565, https://doi.org/10.1594/PANGAEA. 940744, https://doi.pangaea.de/10.1594/PANGAEA.941125. For chemical sensors, raw sensor readouts were used. The fraction of Atlantic and Polar Water were computed for each sampling event following (24) and reported along with distance below the surface (due to mooring blowdown). Sea ice concentration derived from the Advanced Microwave Scanning Radiometer sensor AMSR-2 (42) were downloaded from the Institute of Environmental Physics, University of Bremen (https://seaice.uni-bremen.de/sea-ice-concentration-amsr-eamsr2). Sentinel 3A OLCI chlorophyll surface concentrations were downloaded from https://earth.esa.int/web/sentinel/ sentinel-data-access. For all satellite-derived data, we considered grid points within a radius of 15 km around the moorings. Similar to van Appen et al. 2021 (43), the analyzed datasets consist of ten environmental values for the two locations, F4 and HG-IV, from 01.01.2017 to 31.12.2018. From this dataset, we retrieved the following variables: water temperature (temp °C), fluorescence chlorophyll concentration from in situ sensor (chl_sens $\sim\mu g\ l^{-1}$), daylight (daylight h), water depth (depth m), ice concentration (iceConc %), ice distance (IceDist to 20% ice concentration km), mixed layer depth (MLD m), partial pressure of CO_2 (pCO_2_conc μatm), O_2 concentration (O_2 _conc μmol l^{-1}), polar-water fraction (PW_frac %).

145 ## DNA-extraction and Illumina amplicon-sequencing of 18S rRNA genes

146 Isolation of genomic DNA was carried out using the PowerWater kit (Qiagen, Germany) following the
147 manufacturer's protocol. Obtained DNA was quantified using Quantus (Promega, USA) and stored at -20 °C.
148 18S rRNA gene fragments from the hypervariable V4 region were amplified by polymerase chain reaction
149 (PCR) with primers 528iF (GCGGTAATTCCAGCTCCAA) and 926iR (ACTTTCGTTCTTGATYRR). illuminaNextV4F
150 (TCGTCGGCA GCGTCAGATGTGTATAAGAGACAGGCGGTAATTCCAGCTCC) and illuminaNextV4R
151 (GTCTCGTGGGCTCG-GAGATGTGTATAAGAGACAGGGCAAATGCTTTCGC) (44). All PCRs had a final volume of 50
152 µL and contained 0.02 U Phusion Polymerase (Thermo Fisher, Germany), the 10-fold polymerase buffer
153 according to manufacturer's specification, 0.8 mM each dNTP (Eppendorf, Germany), 0.2 µM L^{-1} of each
154 primer, and 1 µL of template DNA. PCR amplification was performed in a thermal cycler (Eppendorf,
155 Germany) with an initial denaturation (94 °C, 2min) followed by 35 cycles of denaturation (94 °C, 20 sec),
156 annealing (58 °C, 30 sec), and extension (68 °C, 30 sec) with a single final extension (68 °C, 10 min). The PCR
157 products were purified from an agarose gel 1% [w/v] with the NucleoSpin Gel Kit (Macherey-Nagel,
158 Germany) and Mini Elute PCR Purification kit (Qiagen, Germany). Subsequently, DNA concentrations were
159 determined using a Quantus Fluorometer (Promega, USA). Prior to library preparation, DNA fragments were
160 diluted with TE buffer to a concentration of 0.2 ng μL^{-1}. Libraries were prepared according to the 16S
161 Metagenomic Sequencing Library Preparation protocol, and sequenced using MiSeq (Illumina, USA) in 2x300
162 paired-end runs. Sequence data are available under ENA BioProjects PRJEB43889 and PRJEB43890.
163

164 ## Sequence analysis

165 After primer removal using cutadapt (45), reads were processed into amplicon sequence variants (ASVs)
166 using DADA2 v1.14.1 (41), as described in Wietz et al (46). Briefly, reads were trimmed based on quality
167 profiles, with filtering settings truncLen=c(250, 200), maxN=0, minQ=2, maxEE=*c*(3, 3), and trunc*Q* = 0.
168 Followed by merging (minOverlap= 20) and chimera removal, reads were taxonomically classified using

PR2 v4.12 (47). The herein reported data has been processed in the scope of autonomous eDNA biodiversity analyses within the FRAM Observatory, as described under https://github.com/matthiaswietz/FRAM-RAS_eDNA.

Analysis strategy and R packages

All calculations were performed in R version 4.1.3 (2022-03-10). The complete analysis pipeline is available at https://gitlab.com/qtb-hhu/qtb-sda/framstrait_1718. Analysis and plotting tools used for this work are available in a git repository with scripts and an R package. Fourier decomposition was performed with the segmenTier R package (48), available at https://cran.r-project.org/package=segmenTier. The dynamics of eukaryotes were analyzed using the Fourier-transformed time series signals of the relative abundance information. As part of biodiversity, relative species abundance refers to the extent to which a species is common or rare relative to other species in a particular location or community (49). Relative abundance is the percentage composition of an organism of a given species relative to the total number of organisms in that habitat. The data were interpolated on daily bases.

Time series analysis

Each amplicon sequence variant extracted the time series signal from the relative abundance data using a Fourier approach implemented in the R package segmenTier / segmenTools (50). Fourier transformation is a technique for decomposing functions or signals in the sum of their frequency components, characterized by sine and cosine functions. The Fourier Theorem states that any function can be rewritten as the sum of sinusoidal functions. The approximation becomes more accurate with each additional series element. These elements are called Fourier components.

A measurement for seasonality s for the times series t was calculated by the following formula:

Formula1.png

193

194 where f_i is the i-th fourier component of the times series t and abs is the absolute value function(51, 52).

195 After the Fourier transformation, the frequency, amplitude, and phase information of each particular ASV
196 time signal was extracted. These values indicate the seasonality, abundance strength, and time of
197 occurrence within the measured period. The choice for the parameter N = 10, the number of clusters for
198 both locations, was chosen to keep the cluster comparable. The metric (Bayesian Information Criterion -
199 BIC) of the applied clustering algorithm proposes a value around 9 and 10 as the optimal cluster number.
200 Groups of species with similar time signals were identified by a clustering approach in the segmenTools R
201 package (50). The significance of overlapping clusters (shared members by two clusters), illustrated as a
202 color gradient, is calculated based on the negative logarithm of the p-value and the number of overlapping
203 features. All identified clusters were classified into low-light, high-light, and mixed-light clusters depending
204 on the light conditions in which their members show the highest abundance. Further, all clusters were
205 named depending on the mooring (H for HG-IV and F for F4) and numbered in ascending order depending
206 on the phase of the sinusoidal function, which was calculated for each cluster from the average of the
207 cluster members. Therefore, the order of the numbers indicates the order of occurrence within the year.

208

209 **Conditions preference**

210 To determine population prosperity per year, we calculated the sum of all relative abundances for each ASV
211 within a defined time range. The total abundance values were calculated for F4 and HG-IV locations,
212 respectively. Next, we removed all entries with zero abundance to avoid division by zero and calculated the
213 abundance quotients of 2017 and 2018 and vice versa. Based on the calculated quotients, we defined the
214 preferred condition for each ASV, meltwater regime (MWR), and mixed layer regime (MLR) if the
215 log2(quotient) value is >=1 and accordingly -1. ASV that do not fulfill either condition is assigned to the

unspecified group. As a measure of the difference between the locations in a given year for a given group of ASVs, we define the following four quotients:

Formula2_3.png

where X = (F417, F418), Y = (HG-IV17, HG-IV18), and MWR (MLR) containing all MWR (MLR) ASVs relative two-year abundances. The restriction is defined by selecting only the AS abundances from the given time and location.

- p(F42017, HG-IV2017) correspond to the ratio of F4 to HG-IV for species preferring the meltwater regime in 2017.
- p(F42018, HG-IV2018) correspond to the ratio of F4 to HG-IV for species preferring the meltwater regime in 2018.
- t(F42017, HG-IV2017) correspond to the ratio of F4 to HG-IV for species preferring the mixed layer regime in 2017.
- t(F42018, HG-IV2018) correspond to the ratio of F4 to HG-IV for species preferring the mixed layer regime in 2018.

To compare how much the meltwater regime is favored on average versus a mixed layer regime within a given site, we define the following equations:

Formula4.png

where Z = (F417, F418, HG-IV17, HG-IV18), and MWR (MLR) containing all MWR (MLR) ASVs relative two-year abundances. The restriction is defined by selecting only the AS abundances from the given time and location and $_{i}$MWR ($_{j}$MLR) is the i-th (j-th) relative two-year abundance from the MWR (MLR) ASV.

- q(F42017) corresponds to the ratio for meltwater preference over mixed-layer in 2017 at station F4.
- q(F42018) corresponds to the ratio for meltwater preference over mixed-layer in 2018 at station F4.
- q(HG-IV2017) corresponds to the ratio for meltwater preference over mixed-layer in 2017 at station HG-IV.
- q(HG-IV2018) corresponds to the ratio for meltwater preference over mixed-layer in 2018 at station HG-IV.

Cross-condition analysis

To investigate how the dynamics of a particular ASV with a preference for a specific water regime change under the conditions of the opposite water regime, we determined and compared the area under the curve (AUC) from the relative abundance within a time range of 365 days. For that, we used on a daily level interpolated abundance data to which we applied a polynomial function and calculated the AUC for each year separately. Afterward, we compared the ratio of the AUC values between the years to illustrate prosperity differences that are related to the environmental conditions of the individual year.

RESULTS AND DISCUSSION

Environmental conditions

A pronounced extension of the ice edge/MIZ into the WSC during the first half of 2017, compared to 2018, led to different environmental conditions in this part of the eastern Fram Strait. That mixed layer regime was similar to that expected for a seasonally ice-free Arctic Ocean, impacted by Atlantification. More specifically, eastern Fram Strait experienced extended sea ice melt during spring and early summer 2017. According to van Appen et al. 2021 (34), there were significant differences in environmental conditions between 2017 and 2018, with station HG-IV exhibiting more pronounced differences compared to the pure Atlantic Water station F4. This is best reflected by variability in the fraction of Polar Water, distance to the ice edge, ice concentration, and water column stratification (Figure 2).

At HG-IV, the mixed layer depth was overall shallower from January to May 2017 compared to 2018 and F4 due to higher ice concentrations. Moreover, HG-IV was frequently impacted by the intrusion of Polar Water (PW) throughout the annual cycle, which is common for this region. Higher fractions of PW were observed for the period's March, July to August, and November-December of 2017 compared to 2018, according to the RAS data. The intrusion of PW led to lower water temperatures. At HG-IV, temperatures were lower in spring 2017 compared to 2018—ice distances, defined as the distance to 20% ice coverage. At HG-IV, the distance to the ice edge was shorter in 2017 than in 2018 until August but was similar during the remaining months (Figure 2). From mid-August to November; water temperatures were higher in 2017 compared to 2018. In 2017, there was higher ice cover in Fram Strait and subsequent ice melt, resulting in the bloom phenology occurring in a meltwater-stratified water column (MWR). In contrast, in 2018, the bloom phenology occurred in a meltwater-dominated regime (MLR) (34).

At F4, ice distances were not significantly different between the two years. However, water temperatures were higher in 2017 compared to 2018 from mid-August to November.

281 In the following, we investigated the behavior of eukaryotic microbes under different water
282 regimes (melt water and mixed layer). For that, we used a top-down structure to describe the
283 abundance changes over time for i) all ASVs, ii) specific ASV clusters, and iii) single key species.

284

285 **Preference of eukaryotic microbes for the different water regimes**

286 There is a remarkable similarity in ASV composition at both stations. 50% (583) of the ASVs were
287 detected at these two stations, while 22% were unique to F4 (254 ASVs) and 28% to HG-IV (320 ASVs)
288 (Figure S6, Figure S2). Considering the number of ASVs at each station as a baseline, 583 (64.56%) of
289 the 903 ASVs found at HG-IV were also detectable at F4. Conversely, 583 (69.65%) of the 837 ASVs at
290 F4 were present at HG-IV. To analyze the taxa peak abundance of the microbial eukaryotes under
291 different regimes at HG-IV, the total relative abundance for each ASV per year was calculated and
292 compared between the years. Based on that rate, the ASVs were sorted into three groups: the
293 unstratified mixed layer regime (MLR), the highly stratified meltwater regime (MRW), and an
294 unspecified group. The MLR group includes all ASVs (called temperate taxa), which were two times
295 more abundant in HG-IV-2018 compared to HG-IV-2017 (n=67 [11.49% of the shared ASVs]). In
296 contrast, ASVs that were two times more abundant in HG-IV-2017 compared to HG-IV-2018 are
297 members of the MWR group (n=94 [16.12% of the regime shared ASVs]), which were named polar
298 taxa. The remaining ASVs were sorted into an unspecific group (n=422 [72.38% of the regime-shared
299 ASVs]). The last group was excluded from the following analysis. Notably, out of the 583 shared ASVs,
300 only 161 were regime specific in this study, which are distributed between the groups MLR (41.61 %)
301 and MWR (58.38 %) [Table S5].

302

303 We compared both groups to identify differences attributed to either location (as shown in Figure 1)
304 or the varying conditions between 2017 and 2018. To do so, we conducted two types of comparisons:
305 i) within each year, we compared the stations to each other, and ii) within each station, we compared
306 the data from 2017 and 2018. First, we compared the relative abundance differences in 2017

307 between stations. Therefore we calculated the median of the MLR group and MWR group,
308 respectively, for F4 and HG-IV and compared them with each other. Our results showed that the
309 median differences of species favoring mixed-layer were 1.54 times larger than the median
310 differences of the species favoring meltwater in 2017 (Table S5; see methods formula (2,3)). In
311 addition, we could confirm the same observation when comparing the relative abundances of each
312 ASV member of the above groups (one-sided Kolmogorov-Smirnov test p-value: 3.13E-05). In the next
313 step, we repeated the same analysis for the year 2018.
314
315 In contrast to 2017, the median differences in 2018 of the meltwater-favoring species were 2.78
316 times greater than the median differences of the mixed-layer favoring species (Table S5; see methods
317 formula (2,3)). Also, in this case, comparing the relative abundance of the corresponding ASVs could
318 support this observation (one-sided Kolmogorov-Smirnov test p-value: 1.376E-14). Once we had
319 distinguished dissimilarities among the stations, our attention turned to describing dissimilarities
320 over the years. This was motivated by the different water regimes observed in 2017 and 2018 (34).
321 Consequently, this examination enabled us to demonstrate how species abundance is influenced by
322 varying environmental circumstances. Therefore we compared the relative abundance ratio within
323 the same group (MLR, MWR) but between years (2017 vs. 2018). The difference between the two
324 years (2017 and 2018) for each group was less significant at station F4 (MWR=1.23 and MLR=0.60),
325 whereas at HG-IV, the discrepancy was approximately four times higher than that observed at F4 for
326 the same years (MWR=2.13 and MLR=0.27), see Table S5. As a result, we used station F4 as a
327 reference for the constant environment because it is less influenced by meltwater conditions. In
328 contrast, the HG-IV location offers the opportunity to study the effects of Atlantification in a
329 seasonally ice-covered Arctic Ocean, conditions that are expected for the CAO in the near future (53).
330 For that, we examined how each other's water regimes affected the relative abundance of the
331 respective ASV. We aimed to determine whether polar or temperate ASVs were more resilient to the
332 opposing condition. For the analysis, we specifically selected ASVs that are known to grow in polar or
333 temperate conditions (54, 55, 56, 57, 58, 59, 60, 61).

334

335 **Seasonal succession of eukaryotic microbes**

336 To understand the seasonal succession of eukaryotic microbes, we analyzed the phases obtained
337 from the sinusoidal function after Fourier transformation. This allows us to determine the
338 chronological timeline of the species in this region. Community detection from the time series
339 analysis of 837 and 903 ASVs from the F4 and HG-IV moorings revealed ten clusters of seasonally
340 concerted and ordered occurrences of eukaryotic microbial species (Figure 4, Table 1) throughout the
341 observation period. The frequency obtained from the sinusoidal function (light grey) shows the
342 number of high abundance periods of each community per year. Most clusters (85%) had two
343 maxima, indicating that most organisms exhibit a seasonal occurrence with the highest abundance
344 once a year (Figure 4, Table 1). We divided the clusters based on their high abundance period into
345 two classes of light conditions. The low-light (LL 0-2 hours sunlight per day) clusters include species
346 with a high abundance phase in the low-light period from October to March when water temperature
347 and distance to the ice edge are low. The high-light class (HL 2-24 hours sunlight per day) includes
348 clusters, in which the high abundance phases coincide with the high-light period from March to
349 October. All other clusters are collected in the mixed light (NA) class. This distinction allowed us to
350 test the succession of the organisms regarding environmental factors per light condition separately.
351 Next, we compared the species distribution between the two moorings in terms of abundance and
352 seasonality to first test for commonalities and differences between both sampling sites and second,
353 to measure the succession and prosperity of common species regarding the different water regimes.
354 In addition, we compared the time series cluster composition from HG-IV and F4 with each other to
355 identify overlapping communities between both locations. For example, the similarity in cluster
356 composition between the two moorings was highest during the high-light period, particularly
357 between clusters H-06 and F-06 and clusters H-08 and F-08 (Figure 5). The presence of these
358 common ASVs at both mooring sites can be explained by a similar trend in the transportation of
359 temperate organisms through the northward-flowing warmer Atlantic and the transportation of polar

360 organisms through the intrusion of polar water from EGC. This pattern was also observed for
361 zooplankton (62, 63). On the other hand, the varying quantities of ASVs reaching each station
362 because of variations in the influence of the two currents may also explain the biodiversity observed
363 at these two locations (Figure S1).
364

365 **Low-light period**

366 From October to March, the low-light period was characterized by the ordered appearance of four
367 clusters at each mooring (F4: F-01, F-02, F-03, F-04; HG-IV: H-02, H-03, H-04). At both stations,
368 these clusters contained ~40% of the total ASVs, and ~50 % of the total reads. The clusters were
369 dominated by heterotrophic dinoflagellates, parasitic Syndiniales, and other small heterotrophic
370 flagellates like MAST and Picozoa (Figure S4) This mainly heterotrophic community composition
371 resembles prior reports of microbial diversity for the low light period in the Arctic Ocean (63, 64,
372 65) possibly linked to feeding on bacteria (64). However, in all low-light clusters a set of diatom
373 ASVs are present, which possess considerable relative abundances at both stations (Figure S4).
374 The relative sequence abundances of these ASVs were higher at HG-IV than at F4. These ASVs are
375 ice-associated genera or species, such as *Melosira arctica*, *Navicuales sp.,* or *Attheya*
376 *sepentrionalis* (Figure S4 Table S4). Members of these taxa are adapted to low light conditions and
377 colder temperatures (66). They usually live in or under the ice (67). Thus physical exchange
378 processes at the interface between water and sea ice and advection might have been the sources
379 of these diatoms in the water column during winter at HG-IV. The persistence of diatoms
380 (Bacillariophyceae) during the polar night in ice-covered waters was previously observed in the
381 CAO (64) and in a year-round molecular study of eukaryotic microbes in Isfjorden (West
382 Spitsbergen) (65). However, their survival strategies and ecological roles during winter remain
383 primarily unresolved (65). Resting stages such as spores or cysts are a potential strategy of
384 Bacillariophyceae and Dinophyceae to persist in unfavorable conditions like the Arctic winter (68).
385 The taxon-specific survival of diatoms during winter in and under the ice is thought to drive the

386 composition of Arctic phytoplankton during early spring. Diatoms maintain chlorophyll in their
387 cells during the polar night, which gives them a growth advantage at the time of light return (69),
388 when diatoms are the major primary producers in Arctic marine ecosystems.

389

390 **High-light period**

391 The high-light period (March to October) was characterized by a consecutive appearance of three
392 clusters at F4 (F-06, F-08, F-10) and six clusters at HG-IV (H-05, H-06, H-07, H-08, H-09, H-10),
393 respectively (Table 1). The high-light clusters contained ~50 % of all mooring specific ASVs
394 (Table 1). The member composition of the earlier high-light clusters H-05, H-06, and H-07 in 2017 was
395 similar to the composition of the earlier high-light clusters F-06, F-08, and F-10 in 2018 (Figure 5). This
396 suggests that both stations shared a similar community at the beginning of the high-light period
397 (Table S3, Table S4). During this period, sequences of diatoms and other autotrophic taxa, either
398 dominated or were highly abundant besides dinoflagellates (Figure S4, Table S3). Regarding the order
399 of the sequential appearance of the diatoms over the year, we first compared the clusters with ASVs
400 that showed an increased abundance during spring (H-05 and F-06). At HG-IV, diatom ASVs were
401 largely affiliated with the Arctic diatoms *Fragilariopsis cylindrus, Bacillaria paxilifer, Chaetoceros*
402 *neogracilis* and *Grammonema striatula* (70, 71, 72) (Table S3) Their major contribution to the
403 pelagic spring bloom was in line with previous observations (28, 73, 74) emphasizing the polar
404 character of the spring bloom community at HG-IV. The polar taxa *Grammononema*
405 *striatula* and *Chaetoceros neogracilis* were also highly abundant in cluster F-06 (constituting 22% of
406 the total cluster abundance), the first high-light cluster of station F4. In contrast, the temperate
407 taxon *Odontella aurita (75)* was among the five most abundant diatoms (constituting 6% Table S4 F-
408 06) observed in this cluster. The presence of *Odontella aurita* illustrates the influence of Atlantic
409 Water and the concurrent advection of organisms from more temperate waters at this station (Figure
410 6). *Odontella aurita* is also known to be a major contributor to spring blooms in the German Bight
411 (76).

412

413 Differences in diatoms composition between F4 and HG-IV were even more pronounced in the late
414 summer clusters (H-08 and F-10), having their highest abundance after July. At HG-IV, cluster H-08
415 was dominated by sea-ice-associated diatoms such as *Melosira arctica* and other ice-related taxa (67)
416 such as *Fragillariopsis sublineata* and *Fragillariopsis cylindrus*, *Chaetoceros rostratus*, or *Thalassiosira*
417 *sp.* which contribute with 57% (Table S4 H-08) of the total diatom abundance. In contrast, the diatom
418 community in the late cluster F-10 was dominated by *Pseudonitzschia sp* (contributing 38% of the
419 total diatom abundance Table S4 F-10), while the polar taxa that dominated cluster H-08 were only
420 present with smaller contributions. Moreover, this cluster contained significant amounts of *Corethron*
421 *hystrix* and *Proboscia alata* (2% of the total abundance of the diatoms Table S4 F-10, Top11). Those
422 two species thrive in temperate waters (77, 78) illustrating the impact of Atlantic advection at station
423 F4. In cluster H-09, which accounted for 28% of the total abundance in Table S3, the genus
424 Pseudonitzschia was the dominant species. Additionally, in the second cluster at HG-IV (H-02),
425 Pseudonitzschia contributed to a bloom occurring later in the year, specifically in the autumn season
426 (79). Studies have shown that this diatom undergoes blooming throughout the year, typically
427 exhibiting a minor bloom in June, followed by a more substantial bloom in late August or early
428 September (79). Peak sequence abundances of other major Arctic pelagic autotrophs such
429 as *Phaeocystis sp.*, *Chaetoceros socialis* or *Micromonas sp.* were mainly restricted to high-light
430 clusters (Table S3). Notably, sequence contributions represented by ASVs of *Phaeocystis*
431 *pouchetii* were highest in the early spring clusters (H-05 & F-06) accounting for 16 % and 11% of the
432 total abundance respectively (Table S3 H-05, F-06). This result agrees with previous observations in
433 the WSC and under the ice north of Svalbard (80, 81). Nonetheless, *Phaeocystis sp.* and *Micromonas*
434 *sp.* were found even during winter. Their relative contributions to the eukaryotic microbial
435 community remained below levels observed in other molecular genetic studies of the deep
436 chlorophyll maximum (DCM) in the Fram Strait during summer (82). Although there may be ecological
437 reasons for the under-representation of small taxa in this study, the possibility that RAS was biased
438 towards larger eukaryotic microbial cells can not be ruled out.

Impact of sea-ice melt on seasonal phytoplankton dynamics and consequences for bloom phenology in Atlantic waters

The different environmental conditions observed in 2017 and 2018 did not seem to affect the order of the annually recurring community clusters at F4 and HG-IV. Instead, changes in environmental conditions resulted in differences in their persistence, abundance amplitude, and integrated abundances (Figure 4A, Figure 4B). At F4, environmental conditions during the high light periods of 2017 and 2018 were similar. In consequence, the integrated seasonal cluster abundance, reflected by the area under the curve, did not significantly change from one year to the other (Table 1). In contrast, we observed differences between both years for HL and LL periods at HG-IV (Figure S5). According to our data, the changes in environmental conditions, associated with sea-ice melt in spring and summer 2017 at HG-IV, might have significantly affected the communities during high-light periods. For example, these changes can be observed in the high-light cluster H-09 (Table 1). The last period of the cluster (2018) shows a 1.7-fold decrease in abundance compared to the first period (2017). Despite the area under the curve of the early high-light clusters (H-05, H-06, H-07) showing almost no difference between the two years at HG-IV, the amplitude was much lower in 2017 compared to 2018 (Table S2). This observation suggests that the growth rates in 2017 were lower. It is important to note that the organism abundances only reflect relative proportions of the filtered samples. However, in 2017 the RAS was below the productive layer for at least the first half of the high-light period (37), which may explain the lower relative abundances.

Polar pelagic taxa, such as *Chaetoceros neogracilis* and *Grammonema striatula*, were dominant (compared to other Bacillariophyta) in the first clusters of the high-light period at both stations (H-05, F-06, Table S3). These species are more robust to variation in ice coverage. In contrast, the contribution of *Fragillariopsis cylindrus* to the spring cluster H-05 was greater at HG-IV than at F-06, as indicated in Table S3. During the spring of 2017 at HG-IV, lower relative abundances of *Fragilariopsis cylindrus* may suggest lower growth rates, which could be attributed to higher ice

coverage at this station. *Fragilariopsis cylindrus* and *Bacillaria pacillifer* were among the ASVs with the ten highest relative abundances at both stations. They had higher relative abundances during the spring at HG-IV compared to F4 in the observation period, as shown in Table S4 and Figure 6. This was likely because they benefited from lower ice concentrations and comparatively higher water temperatures at HG-IV during the spring of 2018 compared to 2017 (Figure 6). This observation suggests that these polar taxa are not strictly dependent on polar conditions and can tolerate or benefit from Atlantic influence.

Odontella aurita, a temperate taxon occurring at both stations, benefits at both stations from warmer temperatures. The contribution of this temperate species in cluster H-05 was negligible, accounting for only 1% of total abundance, with a further decrease in 2017 to 0.81%, indicating that it struggles to thrive under the ice. In contrast, at mooring F4, its contribution to the spring cluster F-06 was high in both years (Table S3) as temperatures were in a similar range. During the later part of the season in HG-IV, the area under the curve of cluster H-08 showed a 1.5-fold increase in 2017 compared to 2018, as indicated in Table 1. This cluster mainly comprised typical sea-ice-associated diatoms like *Melosira arctica*, *Fragillariopsis sublineata* and *-cylindrus*, and *Chaetoceros rostratus*. Interestingly, these diatoms did not contribute significantly to the phytoplankton community at F4 during the same time of the year. This indicates a sea-ice melt-related release of sea-ice-associated taxa. The environmental conditions existing at this time, especially meltwater stratification, promoted their bloom in the Atlantic Water of Fram Strait (Table S3 Table S4).

During the specified time frame, there was a notable decrease in the prevalence of polar spring phytoplankton species at the start of the season, accompanied by a corresponding increase in the abundance of ice-associated phytoplankton species during the autumn of 2017. It is worth noting that the peak abundance of ice-associated phytoplankton species usually occurs later in the season in the CAO (83, 84, 85). Ice-associated phytoplankton is less present at HG-IV in 2018 (ice-free year) and does not significantly contribute to the autumn community at ice-free station F4 in either year.

CONCLUSION

In this study, we compared the dynamics of phytoplankton ASVs from two locations in the Fram Strait (moorings HG-IV and F4) as recorded in 2017 and 2018. Although data from only two years are not necessarily representative of the long-term development of environmental parameters, these particular years exhibit conditions that make them appear ideal for comparing current conditions with those expected in the future in an Atlantified CAO. This comparison supports a new perspective on how the eukaryotic microbial community in the Central Arctic Ocean might change in the near future. Climate change will likely lead to an ice-free Central Arctic Ocean in summer but ice-covered in winter, as suggested by some climate model scenarios (14).

In our analysis, we could show that a meltwater regime can strongly influence arctic micro-eukaryotes on several levels and that phytoplankton bloom phenology in 2017 is a result of increased sea ice melt (34). We could extend previous observations about the influence of sea-ice melt on community dynamics and carbon export. We propose that sea ice melt and the resulting environmental conditions are putative key drivers of microbial eukaryotic community composition and bloom phenomenology. Our observations suggest that polar pelagic and ice-associated taxa (such as *Fragilariopsis cylindrus* or *Melosira arctica*) are relatively tolerant of more Atlantic oceanographic conditions. In contrast, temperate taxa (such as *Odontella aurita* or *Proboscia alata*) have limited potential to persist in colder ice-impacted waters. Thus, we hypothesize that sea-ice melt in the MIZ may hinder the northward expansion of temperate Atlantic taxa towards the CAO. This trend will continue even as Atlantic oceanographic conditions move further northwards.

ACKNOWLEDGEMENTS

We thank Theresa Hargesheimer, Jana Bäger and Daniel Scholz for technical support of the RAS deployment. Moreover we thank the captains and crews of RV Polarstern for excellent support at sea, and the chief scientists for leading the various expeditions conducted for this study. Ship time for RV Polarstern was provided under grants AWI_PS99_00, AWI_PS100_01, AWI_PS107_05, AWI_PS114_01, AWI_PS121_01 of RV Polarstern. Our special thanks go to S. Neuhaus for bioinformatic support, K. Oetjen and S. Ziemann for excellent technical support in the laboratory, Eva-Maria Nöthig for critical reading of the manuscript, Martina Löbl for coordination of the FRAM-project.

AUTHOR CONTRIBUTIONS

EO conducted the data analyses. WJvA, CB, MW, STV and KM are responsible for the sampling design. STV contributed nutrient data. WJvA contributed oceanographic data. EO, KM and OP interpreted the data, conceptualized the and drafted the manuscript. All authors contributed to improving the final manuscript, by contributions to the scientific interpretation of the data and the discussion of results.

FUNDING

This study was accomplished in the framework of the HGF Infrastructure Program FRAM and institutional funds of the Alfred-Wegener-Institute Helmholtz Centre for Polar and Marine Research. This work was further supported by The Deutsche Forschungsgemeinschaft (DFG) under grant number EB 418/6-1 (From Dusk till

Dawn) and under Germany's Excellence Strategy - EXC-2048/1 - project ID 390686111 (CEPLAS)(EO and OE).

COMPETING INTERESTS

The authors declare no competing interests.

Data Availability Statement

The datasets generated during and/or analysed during the current study are available in the gitlab repository, https://gitlab.com/qtb-hhu/qtb-sda/framstrait_1718.

ADDITIONAL INFORMATION

Correspondence and requests for materials should be addressed to Ellen Oldenburg.

References

1. Rantanen M, Karpechko AY, Lipponen A, Nordling K, Hyvärinen O, Ruosteenoja K, et al. The Arctic has warmed nearly four times faster than the globe since 1979. Communications Earth & Environment. 2022;3(1):168.

2. Zhang L, Risser MD, Molter EM, Wehner MF, O'Brien TA. Accounting for the spatial structure of weather systems in detected changes in precipitation extremes. Weather and Climate Extremes. 2022;38:100499.

3. Perovich D, Smith M, Light B, Webster M. Meltwater sources and sinks for multiyear Arctic sea ice in summer. The Cryosphere. 2021;15(9):4517-25.

4. Richter-Menge J, Jeffries M, Osborne E. 5. THE ARCTIC. Bulletin of the American Meteorological Society. 2018;99(8):S143-S.

5. Kwok R. Arctic sea ice thickness, volume, and multiyear ice coverage: losses and coupled variability (1958–2018). Environmental Research Letters. 2018;13(10):105005.

6. Asbjørnsen H, Årthun M, Skagseth Ø, Eldevik T. Mechanisms underlying recent Arctic atlantification. Geophysical research letters. 2020;47(15):e2020GL088036.

7. Wassmann P, Duarte CM, Agusti S, Sejr MK. Footprints of climate change in the Arctic marine ecosystem. Global change biology. 2011;17(2):1235-49.

8. Dalpadado P, Ingvaldsen RB, Stige LC, Bogstad B, Knutsen T, Ottersen G, et al. Climate effects on Barents Sea ecosystem dynamics. ICES Journal of Marine Science. 2012;69(7):1303-16.

9. Fossheim M, Primicerio R, Johannesen E, Ingvaldsen RB, Aschan MM, Dolgov AV. Recent warming leads to a rapid borealization of fish communities in the Arctic. Nature Climate Change. 2015;5(7):673-7.

10. Kortsch S, Primicerio R, Fossheim M, Dolgov AV, Aschan M. Climate change alters the structure of arctic marine food webs due to poleward shifts of boreal generalists. Proceedings of the Royal Society B: Biological Sciences. 2015;282(1814):20151546.

11. Polyakov IV, Pnyushkov AV, Alkire MB, Ashik IM, Baumann TM, Carmack EC, et al. Greater role for Atlantic inflows on sea-ice loss in the Eurasian Basin of the Arctic Ocean. Science. 2017;356(6335):285-91.

12. Vihtakari M, Welcker J, Moe B, Chastel O, Tartu S, Hop H, et al. Black-legged kittiwakes as messengers of Atlantification in the Arctic. Scientific Reports. 2018;8(1):1-11.

13. Polyakov IV, Alkire MB, Bluhm BA, Brown KA, Carmack EC, Chierici M, et al. Borealization of the Arctic Ocean in response to anomalous advection from sub-Arctic seas. Frontiers in Marine Science. 2020;7:491.

14. Collins M, Knutti R, Arblaster J, Dufresne J-L, Fichefet T, Friedlingstein P, et al. Long-term climate change: projections, commitments and irreversibility. 2013.

15. Flocco D, Feltham DL, Turner AK. Incorporation of a physically based melt pond scheme into the sea ice component of a climate model. Journal of Geophysical Research: Oceans. 2010;115(C8).

16. Horvat C, Tziperman E. A prognostic model of the sea-ice floe size and thickness distribution. The Cryosphere. 2015;9(6):2119-34.

17. Tsamados M, Feltham D, Petty A, Schroeder D, Flocco D. Processes controlling surface, bottom and lateral melt of Arctic sea ice in a state of the art sea ice model. Philosophical Transactions of the Royal Society A: Mathematical, Physical and Engineering Sciences. 2015;373(2052):20140167.

18. Lee CM, Thomson J, Zone MI, Teams ASS. An autonomous approach to observing the seasonal ice zone in the western Arctic. Oceanography. 2017;30(2):56-68.

19. Strong C, Foster D, Cherkaev E, Eisenman I, Golden KM. On the definition of marginal ice zone width. Journal of Atmospheric and Oceanic Technology. 2017;34(7):1565-84.

20. Boutin G, Lique C, Ardhuin F, Rousset C, Talandier C, Accensi M, et al. Towards a coupled model to investigate wave–sea ice interactions in the Arctic marginal ice zone. The Cryosphere. 2020;14(2):709-35.

21. Lester CW, Wagner TJW, McNamara DE, Cape MR. The influence of meltwater on phytoplankton blooms near the sea-ice edge. Geophysical Research Letters. 2021;48(2):e2020GL091758.

22. Pachauri RK, Allen MR, Barros VR, Broome J, Cramer W, Christ R, et al. Climate change 2014: synthesis report. Contribution of Working Groups I, II and III to the fifth assessment report of the Intergovernmental Panel on Climate Change: Ipcc; 2014.

23. Wekerle C, Wang Q, von Appen WJ, Danilov S, Schourup-Kristensen V, Jung T. Eddy-resolving simulation of the Atlantic water circulation in the Fram Strait with focus on the seasonal cycle. Journal of Geophysical Research: Oceans. 2017;122(11):8385-405.

24. von Appen WJ, Wekerle C, Hehemann L, Schourup-Kristensen V, Konrad C, Iversen MH. Observations of a submesoscale cyclonic filament in the marginal ice zone. Geophysical Research Letters. 2018;45(12):6141-9.

25. Hofmann Z, von Appen WJ, Wekerle C. Seasonal and mesoscale variability of the two Atlantic Water recirculation pathways in Fram Strait. Journal of Geophysical Research: Oceans. 2021;126(7):e2020JC017057.

26. Timmermans M-L, Labe Z. Sea surface temperature. 2022.

27. Lind S, Ingvaldsen RB, Furevik T. Arctic warming hotspot in the northern Barents Sea linked to declining sea-ice import. Nature climate change. 2018;8(7):634-9.

28. Lafond A, Leblanc K, Quéguiner B, Moriceau B, Leynaert A, Cornet V, et al. Late spring bloom development of pelagic diatoms in Baffin Bay. Elementa: Science of the Anthropocene. 2019;7.

29. Søreide JE, Pitusi V, Vader A, Damsgård B, Nilsen F, Skogseth R, et al. Environmental status of Svalbard coastal waters: coastscapes and focal ecosystem components. 2020.

30. Reigstad M, Gabrielsen T, Amargant M, Amundsen R, Bluhm B, Bodur Y, et al. Seasonal Cruise Q3: Cruise Report. The Nansen Legacy Report Series. 2022(27).

31. von Eye M, von Eye A, Rodrigues J. Global warming and changes in sea ice in the Greenland Sea: 1979–2007. InterStat: Available online at http://interstat statjournals net/YEAR/2009/abstracts/0905003 php. 2009.

32. Hansen J, Sato M, Russell G, Kharecha P. Climate sensitivity, sea level and atmospheric carbon dioxide. Philosophical Transactions of the Royal Society A: Mathematical, Physical and Engineering Sciences. 2013;371(2001):20120294.

33. Sumata H, de Steur L, Divine DV, Granskog MA, Gerland S. Regime shift in Arctic Ocean sea ice thickness. Nature. 2023;615(7952):443-9.

34. von Appen W-J, Waite AM, Bergmann M, Bienhold C, Boebel O, Bracher A, et al. Sea-ice derived meltwater stratification slows the biological carbon pump: results from continuous observations. Nature Communications. 2021;12(1):7309.

35. Lampe V, Nöthig E-M, Schartau M. Spatio-temporal variations in community size structure of Arctic protist plankton in the Fram Strait. Frontiers in Marine Science. 2021;7:579880.

36. Wingfield JC. Ecological processes and the ecology of stress: the impacts of abiotic environmental factors. Functional Ecology. 2013;27(1):37-44.

37. Kilias E, Wolf C, Peeken I, Metfies K, editors. Picoplankton: The successful spreading over the Arctic Ocean2012.

38. Metfies K, von Appen W-J, Kilias E, Nicolaus A, Nöthig E-M. Biogeography and photosynthetic biomass of arctic marine pico-eukaroytes during summer of the record sea ice minimum 2012. PLoS One. 2016;11(2):e0148512.

39. Fadeev E, Rogge A, Ramondenc S, Nöthig E-M, Wekerle C, Bienhold C, et al. Sea-ice retreat may decrease carbon export and vertical microbial connectivity in the Eurasian Arctic basins. 2020.

649 40. Soltwedel T, Bauerfeind E, Bergmann M, Budaeva N, Hoste E, Jaeckisch N, et al.
650 HAUSGARTEN: multidisciplinary investigations at a deep-sea, long-term observatory in the
651 Arctic Ocean. Oceanography. 2005(3).
652 41. Callahan BJ, McMurdie PJ, Rosen MJ, Han AW, Johnson AJA, Holmes SP. DADA2: High-
653 resolution sample inference from Illumina amplicon data. Nature methods. 2016;13(7):581-
654 3.
655 42. Spreen G, Kaleschke L, Heygster G. Sea ice remote sensing using AMSR-E 89-GHz
656 channels. Journal of Geophysical Research: Oceans. 2008;113(C2).
657 43. von Appen W-J. Report on Mooring Processing of PS99. 2/PS100/PS101 Recoveries.
658 2017.
659 44. Metfies K, Hessel J, Klenk R, Petersen W, Wiltshire KH, Kraberg A. Uncovering the
660 intricacies of microbial community dynamics at Helgoland Roads at the end of a spring bloom
661 using automated sampling and 18S meta-barcoding. Plos one. 2020;15(6):e0233921.
662 45. Martin M. Cutadapt removes adapter sequences from high-throughput sequencing
663 reads. EMBnet journal. 2011;17(1):10-2.
664 46. Wietz M, Bienhold C, Metfies K, Torres-Valdés S, von Appen W-J, Salter I, et al. The
665 polar night shift: seasonal dynamics and drivers of Arctic Ocean microbiomes revealed by
666 autonomous sampling. ISME Communications. 2021;1(1):1-12.
667 47. Guillou L, Bachar D, Audic S, Bass D, Berney C, Bittner L, et al. The Protist Ribosomal
668 Reference database (PR2): a catalog of unicellular eukaryote small sub-unit rRNA sequences
669 with curated taxonomy. Nucleic acids research. 2012;41(D1):D597-D604.
670 48. Machné R, Murray DB, Stadler PF. Similarity-based segmentation of multi-dimensional
671 signals. Scientific Reports. 2017;7(1):12355.

672 49. Hubbell SP. The unified neutral theory of biodiversity and biogeography (MPB-32).
673 The Unified Neutral Theory of Biodiversity and Biogeography (MPB-32): Princeton University
674 Press; 2011.
675 50. Machné R, Murray DB. The yin and yang of yeast transcription: elements of a global
676 feedback system between metabolism and chromatin. PloS one. 2012;7(6):e37906.
677 51. Cooley JW, Tukey JW. An algorithm for the machine calculation of complex Fourier
678 series. Mathematics of computation. 1965;19(90):297-301.
679 52. Lipovetsky S. Numerical Recipes: The Art of Scientific Computing. Technometrics.
680 2009;51(4):481.
681 53. Burki F, Sandin MM, Jamy M. Diversity and ecology of protists revealed by
682 metabarcoding. Current Biology. 2021;31(19):R1267-R80.
683 54. Mock T, Hoch N. Long-term temperature acclimation of photosynthesis in steady-
684 state cultures of the polar diatom Fragilariopsis cylindrus. Photosynthesis research.
685 2005;85:307-17.
686 55. Bayer-Giraldi M, Weikusat I, Besir H, Dieckmann G. Characterization of an antifreeze
687 protein from the polar diatom Fragilariopsis cylindrus and its relevance in sea ice.
688 Cryobiology. 2011;63(3):210-9.
689 56. Raghu Prasad R, Nair P. Observations on the distribution and occurrence of diatoms in
690 the inshore waters of the Gulf of Mannar and Palk Bay. Indian Journal of Fisheries.
691 1960;7(1):49-68.
692 57. Comeau AM, Philippe B, Thaler M, Gosselin M, Poulin M, Lovejoy C. Protists in Arctic
693 drift and land-fast sea ice. Journal of Phycology. 2013;49(2):229-40.

694 58. Tisserand L, Dadaglio L, Intertaglia L, Catala P, Panagiotopoulos C, Obernosterer I, et
695 al. Use of organic exudates from two polar diatoms by bacterial isolates from the Arctic
696 Ocean. Philosophical Transactions of the Royal Society A. 2020;378(2181):20190356.
697 59. Lacour T, Larivière J, Ferland J, Morin P-I, Grondin P-L, Donaher N, et al.
698 Photoacclimation of the polar diatom Chaetoceros neogracilis at low temperature. Plos one.
699 2022;17(9):e0272822.
700 60. Barbieri ES, Villafañ VE, Helbling EW. Experimental assessment of UV effects on
701 temperate marine phytoplankton when exposed to variable radiation regimes. Limnology
702 and Oceanography. 2002;47(6):1648-55.
703 61. Lomas MW, Baer SE, Acton S, Krause JW. Pumped up by the cold: Elemental quotas
704 and stoichiometry of cold-water diatoms. Frontiers in Marine Science. 2019;6:286.
705 62. Kraft A, Berge J, Varpe Ø, Falk-Petersen S. Feeding in Arctic darkness: mid-winter diet
706 of the pelagic amphipods Themisto abyssorum and T. libellula. Marine Biology.
707 2013;160:241-8.
708 63. Egge E, Elferink S, Vaulot D, John U, Bratbak G, Larsen A, et al. An 18S V4 rRNA
709 metabarcoding dataset of protist diversity in the Atlantic inflow to the Arctic Ocean, through
710 the year and down to 1000 m depth. Earth System Science Data. 2021;13(10):4913-28.
711 64. Sherr EB, Sherr BF, Wheeler PA, Thompson K. Temporal and spatial variation in stocks
712 of autotrophic and heterotrophic microbes in the upper water column of the central Arctic
713 Ocean. Deep Sea Research Part I: Oceanographic Research Papers. 2003;50(5):557-71.
714 65. Marquardt M, Vader A, Stübner EI, Reigstad M, Gabrielsen TM. Strong seasonality of
715 marine microbial eukaryotes in a high-Arctic fjord (Isfjorden, in West Spitsbergen, Norway).
716 Applied and environmental microbiology. 2016;82(6):1868-80.
717 66. Cota GF. Photoadaptation of high Arctic ice algae. Nature. 1985;315:219-22.

718 67. von Quillfeldt CH. Distribution of diatoms in the Northeast Water polynya, Greenland.
719 Journal of Marine Systems. 1997;10(1-4):211-40.
720 68. Smetacek V. Role of sinking in diatom life-history cycles: ecological, evolutionary and
721 geological significance. Marine biology. 1985;84:239-51.
722 69. van de Poll WH, Abdullah E, Visser RJ, Fischer P, Buma AG. Taxon-specific dark survival
723 of diatoms and flagellates affects Arctic phytoplankton composition during the polar night
724 and early spring. Limnology and Oceanography. 2020;65(5):903-14.
725 70. Von Quillfeldt C. Common diatom species in Arctic spring blooms: their distribution
726 and abundance. 2000.
727 71. Stachura-Suchoples K, Enke N, Schlie C, Schaub I, Karsten U, Jahn R. Contribution
728 towards a morphological and molecular taxonomic reference library of benthic marine
729 diatoms from two Arctic fjords on Svalbard (Norway). Polar Biology. 2016;39:1933-56.
730 72. Balzano S, Percopo I, Siano R, Gourvil P, Chanoine M, Marie D, et al. Morphological
731 and genetic diversity of Beaufort Sea diatoms with high contributions from the Chaetoceros
732 neogracilis species complex. Journal of Phycology. 2017;53(1):161-87.
733 73. Wassmann P, Ratkova T, Andreassen I, Vernet M, Pedersen G, Rey F. Spring bloom
734 development in the marginal ice zone and the central Barents Sea. Marine Ecology.
735 1999;20(3-4):321-46.
736 74. Lalande C, Grebmeier JM, McDonnell AM, Hopcroft RR, O'Daly S, Danielson SL. Impact
737 of a warm anomaly in the Pacific Arctic region derived from time-series export fluxes. Plos
738 one. 2021;16(8):e0255837.
739 75. Hartley B, Ross R, Williams DM. A check-list of the freshwater, brackish and marine
740 diatoms of the British Isles and adjoining coastal waters. Journal of the Marine Biological
741 Association of the United Kingdom. 1986;66(3):531-610.

742 76. Schlüter MH, Kraberg A, Wiltshire KH. Long-term changes in the seasonality of
743 selected diatoms related to grazers and environmental conditions. Journal of sea Research.
744 2012;67(1):91-7.
745 77. Sukhanova I, Flint M, Whitledge T, Stockwell D, Rho T. Mass development of the
746 planktonic diatom Proboscia alata over the Bering Sea shelf in the summer season.
747 Oceanology. 2006;46:200-16.
748 78. Crawford RM, Hinz F, Honeywill C. Three species of the diatom genus Corethron
749 Castracane: structure, distribution and taxonomy. Diatom Research. 1998;13(1):1-28.
750 79. Bates SS, Garrison DL, Horner RA. Bloom dynamics and physiology of domoic-acid-
751 producing Pseudo-nitzschia species. NATO ASI series G ecological sciences. 1998;41:267-92.
752 80. Nöthig E-M, Bracher A, Engel A, Metfies K, Niehoff B, Peeken I, et al. Summertime
753 plankton ecology in Fram Strait—a compilation of long-and short-term observations. Polar
754 Research. 2015;34(1):23349.
755 81. Kauko HM, Pavlov AK, Johnsen G, Granskog MA, Peeken I, Assmy P. Photoacclimation
756 state of an Arctic underice phytoplankton bloom. Journal of Geophysical Research: Oceans.
757 2019;124(3):1750-62.
758 82. Kilias E, Wolf C, Nöthig EM, Peeken I, Metfies K. Protist distribution in the Western
759 Fram Strait in summer 2010 based on 454-pyrosequencing of 18S rDNA. Journal of
760 Phycology. 2013;49(5):996-1010.
761 83. Biggs TE, Alvarez-Fernandez S, Evans C, Mojica KD, Rozema PD, Venables HJ, et al.
762 Antarctic phytoplankton community composition and size structure: importance of ice type
763 and temperature as regulatory factors. Polar Biology. 2019;42:1997-2015.

84. Dalpadado P, Arrigo KR, van Dijken GL, Skjoldal HR, Bagøien E, Dolgov AV, et al. Climate effects on temporal and spatial dynamics of phytoplankton and zooplankton in the Barents Sea. Progress in Oceanography. 2020;185:102320.

85. Nardelli SC, Gray PC, Stammerjohn SE, Schofield O. Characterizing coastal phytoplankton seasonal succession patterns on the West Antarctic Peninsula. Limnology and oceanography. 2023.

Figures:

Fig1.pdf

Figure 1: **Map of mooring locations, major currents, and water depths in Fram Strait**. The main currents in the area are illustrated schematically: West Spitsbergen Current (WSC) in red and East Greenland Current (EGC) in blue. The locations of the moored remote access samplers discussed in this study are marked in black for HG-IV and F4. F4 is located in the WSC and HG-IV west of the WSC. Land is displayed in gray and the different water depths in a white-blue color gradient.

Fig2.png

Figure 2: **Environmental data for the F4 (dark orange) and HG-IV (blue) location from 2017 to 2018.** The x-axis indicates the period from 01.01.2017 to 31.12.2018. The y-axis indicates: **A:** Mixed layer depth (Minimum of the estimated MLD) [m] **B:** Distance to 20% ice

concentration (*) [m] **C:** Sea ice concentration [%] **D:** Temperature [°C] E: Polar water fraction [%] F: Chlorophyll a concentration (**) [µg L−1] *Negative values indicate that the ice edge is south east of the mooring points at the blue curve March 2017 to September 2017) **Sensor did not work before August 2017.

Fig3.png

Figure 3: Effects of meltwater and mixed layer conditions on temperate (dark green) and polar (light green) taxa. The x-axis shows the months January through December from 2017 through 2018. The green areas reflect the relative abundances of temperate (dark green) and polar (light green) taxa as extracted from the data. Since the data is relative, no quantification is given on the y-axis. The relative abundance curves of A and B were derived from water column samples from cluster F-06, and C and D from cluster H-06. **A:** Polar and temperate taxa are observed in similar abundances in the highly stratified meltwater regime at F4 in 2017. **B:** Similar abundances for polar and temperate taxa in the mixed layer regime at F4 in 2018. **C:** Reduced abundance of temperate taxa in the meltwater regime with high stratification at HG-IV in 2017. **D:** Reduced abundance of polar taxa in the mixed layer regime at HG-IV in 2018.

Fig4.png

Figure 4: **Time-Series Clustering for both moorings spanning the years 2017-2018.** The x-axis indicates the period from 01.01.2017 to 31.12.2018. Black sinusoidal curves show the predicted seasonality of the entire cluster based on the dominant Fourier component. The respective relative abundance is shown for each cluster on the left y-axis. Cluster names are shown on the right. The clusters are sorted by phase which illustrates the time

816 of maximal abundance of each community. Clusters are colored according to the three
817 classes HL (green), LL (grey), and NA (white) introduced in the text. **A:** HG-IV, **B:** F4
818
819 Fig5.png
820
821 Figure 5: **Cluster overlap between F4 and HG-IV locations.** The clusters of F4 are plotted
822 on the y-axis against the clusters of HG-IV. The numbers inside the boxes indicate how
823 many ASVs are shared between two clusters The clusters of each location are sorted
824 according to their classes: low-light (grey box frame), mix-light (white box frame) and
825 high-light (green box frame) from top to bottom (F4) and from left to right (HG-IV). The
826 background color of the boxes shows the significance of the overlap from dark (highly
827 significant) to white (non significant).
828 Fig6.png
829
830 Figure 6: **Correlation between the relative abundances of selected ASVs in 2017 vs 2018:**
831 The diagonal (blue line) indicates the line on which abundances in 2017 and 2018 would
832 be identical. On the left side (first and second columns) selected polar taxa are displayed,
833 where the first column shows the species at HG-IV and the second column the same ASV
834 at F4. The right side shows selected temperate taxa, where the third column displays
835 species at HG-IV and the fourth column the same ASV at F4. The dots indicate:
836 *Fragilariopsis cylindrus* (ASV207: H-08, F-10), *Fragilariopsis cylindrus* (ASV16: H-05, F-02),
837 *Bacillaria paxillifer* (ASV98: H-03, F-06), *Chaetoceros neograciis* (ASV17: H-05, F-06),
838 *Grammonema stratula* (ASV33: H-05, F-06), *Odontella aurita* (ASV96:H-05, F-06),
839 *Corethron hystrix* (ASV172: F-10), *Proboscia alata* (ASV947: F-06), Color bar and colored
840 dots indicate month of the year from blue (winter) to red (summer).

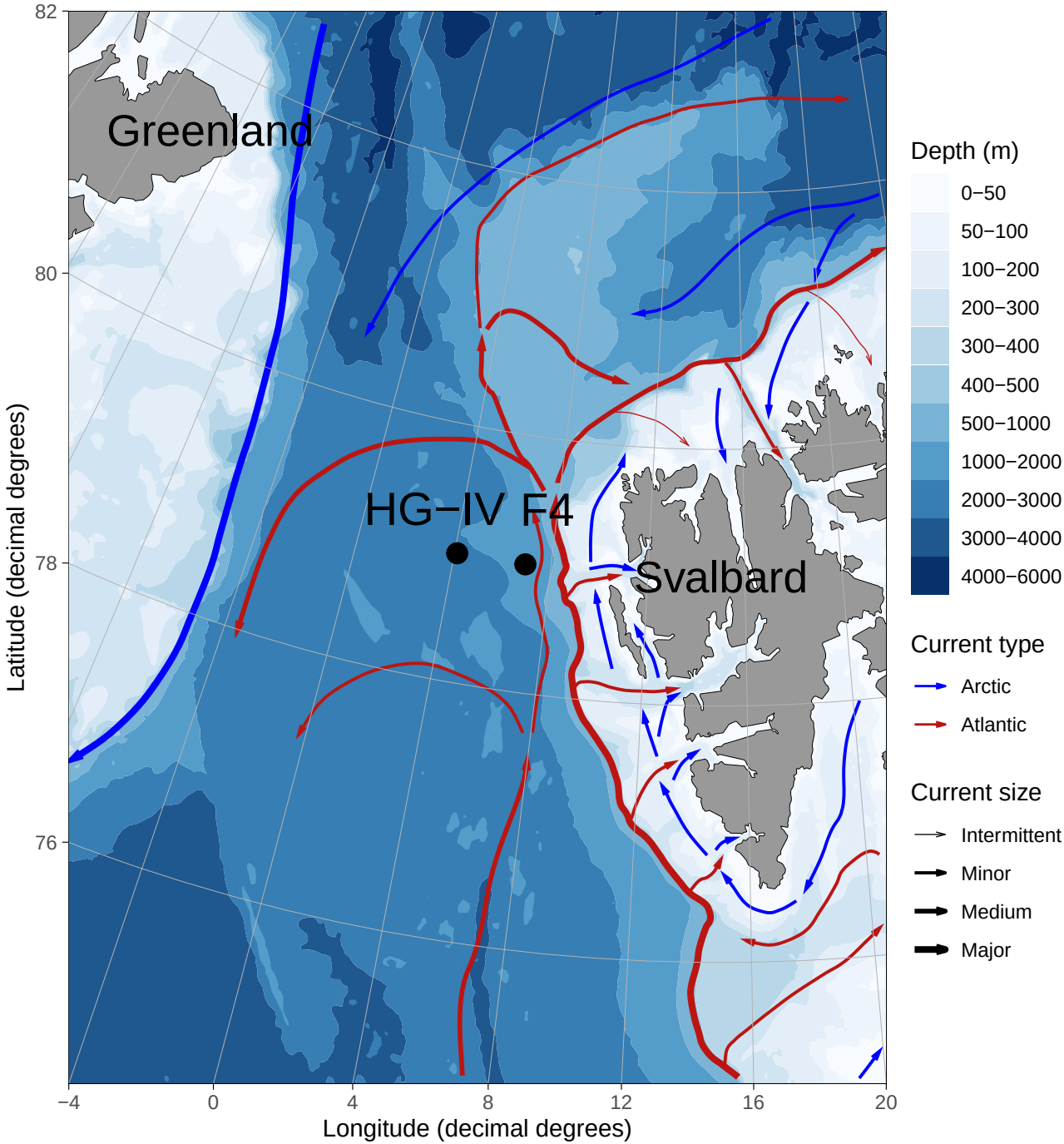
Greenland
HG−IV F4
Svalbard
Latitude (decimal degrees)
Longitude (decimal degrees)
82
80
78
76
−4
0
4
8
12
16
20
Depth (m)
0−50
50−100
100−200
200−300
300−400
400−500
500−1000
1000−2000
2000−3000
3000−4000
4000−6000
Current type
Arctic
Atlantic
Current size
Intermittent
Minor
Medium
Major

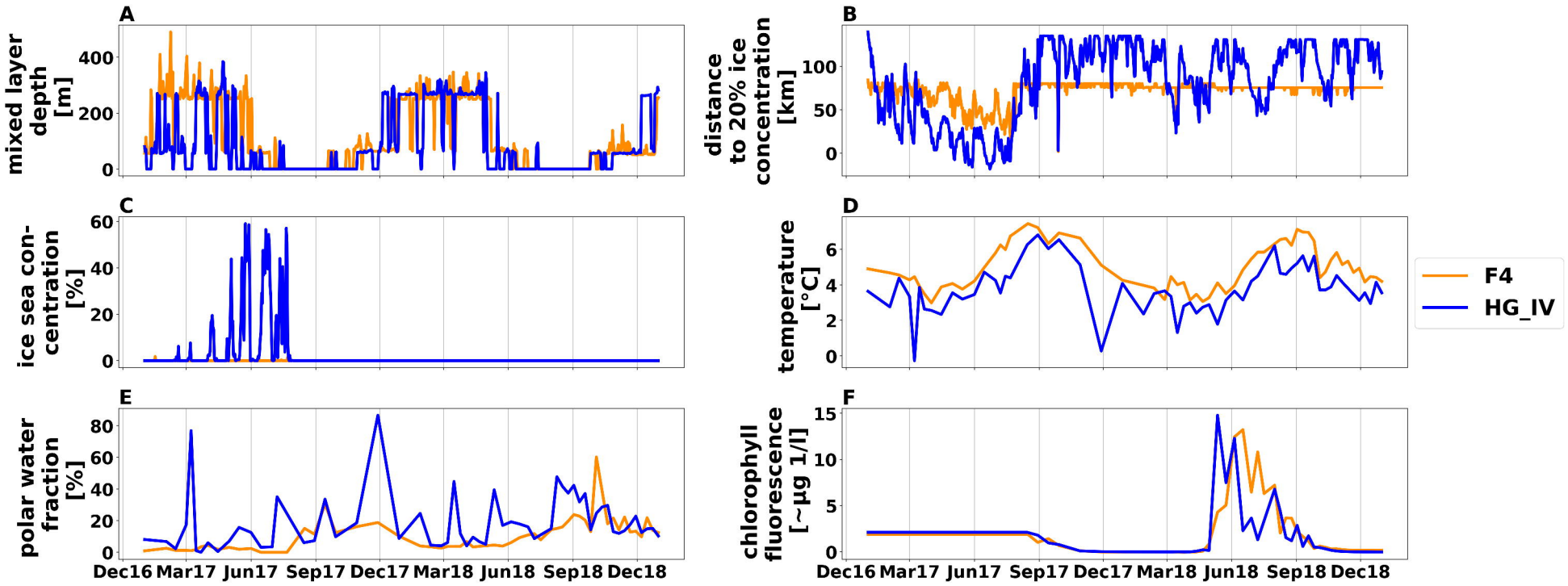
A
mixed layer depth [m]
400
200
0
B
distance to 20% ice concentration [km]
100
50
0
C
ice sea con-centration [%]
60
40
20
0
D
temperature [°C]
6
4
2
0
F4
HG_IV
E
polar water fraction [%]
80
60
40
20
0
F
chlorophyll fluorescence [~µg 1/l]
15
10
5
0
Dec16 Mar17 Jun17 Sep17 Dec17 Mar18 Jun18 Sep18 Dec18
Dec16 Mar17 Jun17 Sep17 Dec17 Mar18 Jun18 Sep18 Dec18

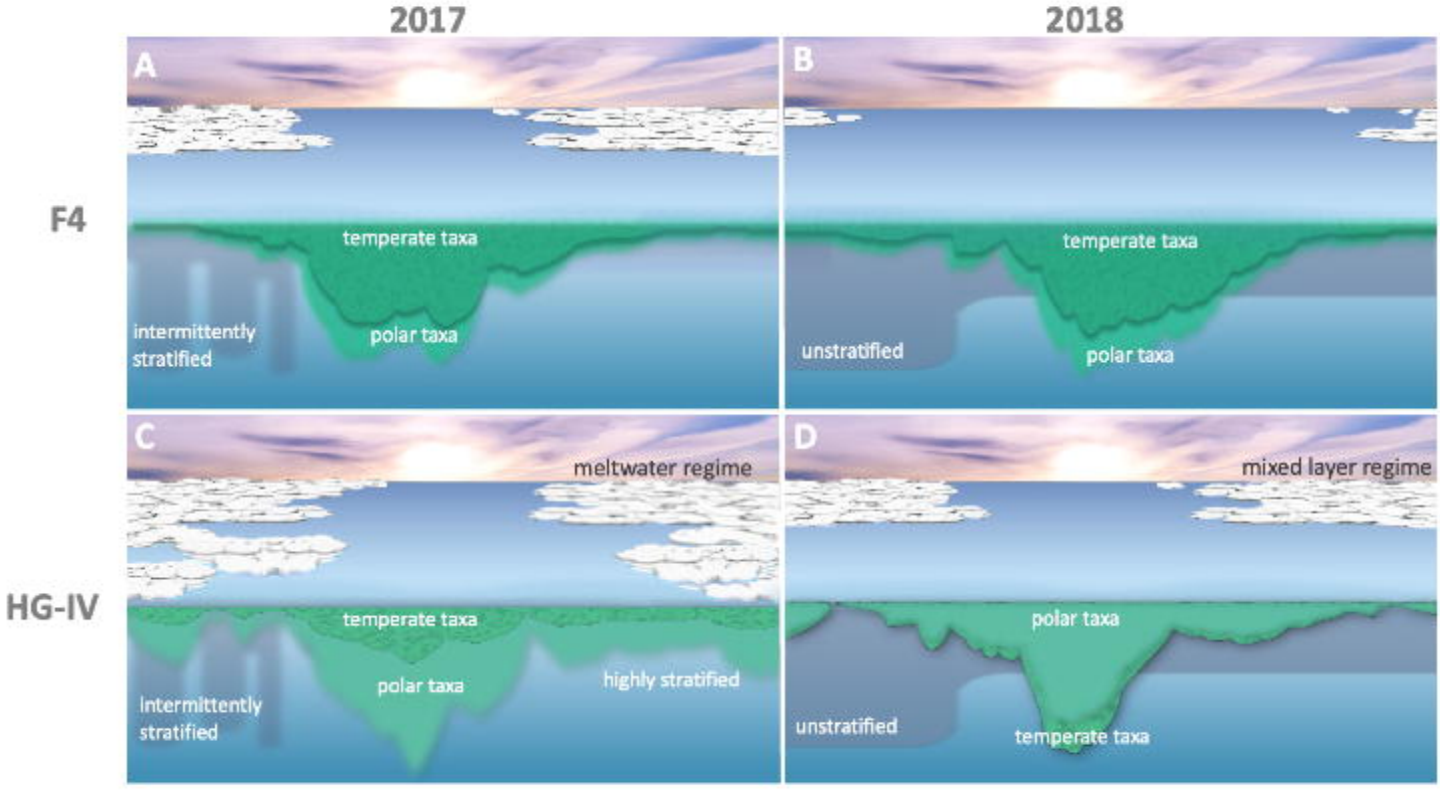
2017
2018
A
B
F4
temperate taxa
intermittently stratified
polar taxa
temperate taxa
unstratified
polar taxa
C
D
meltwater regime
mixed layer regime
HG-IV
temperate taxa
polar taxa
highly stratified
intermittently stratified
polar taxa
unstratified
temperate taxa

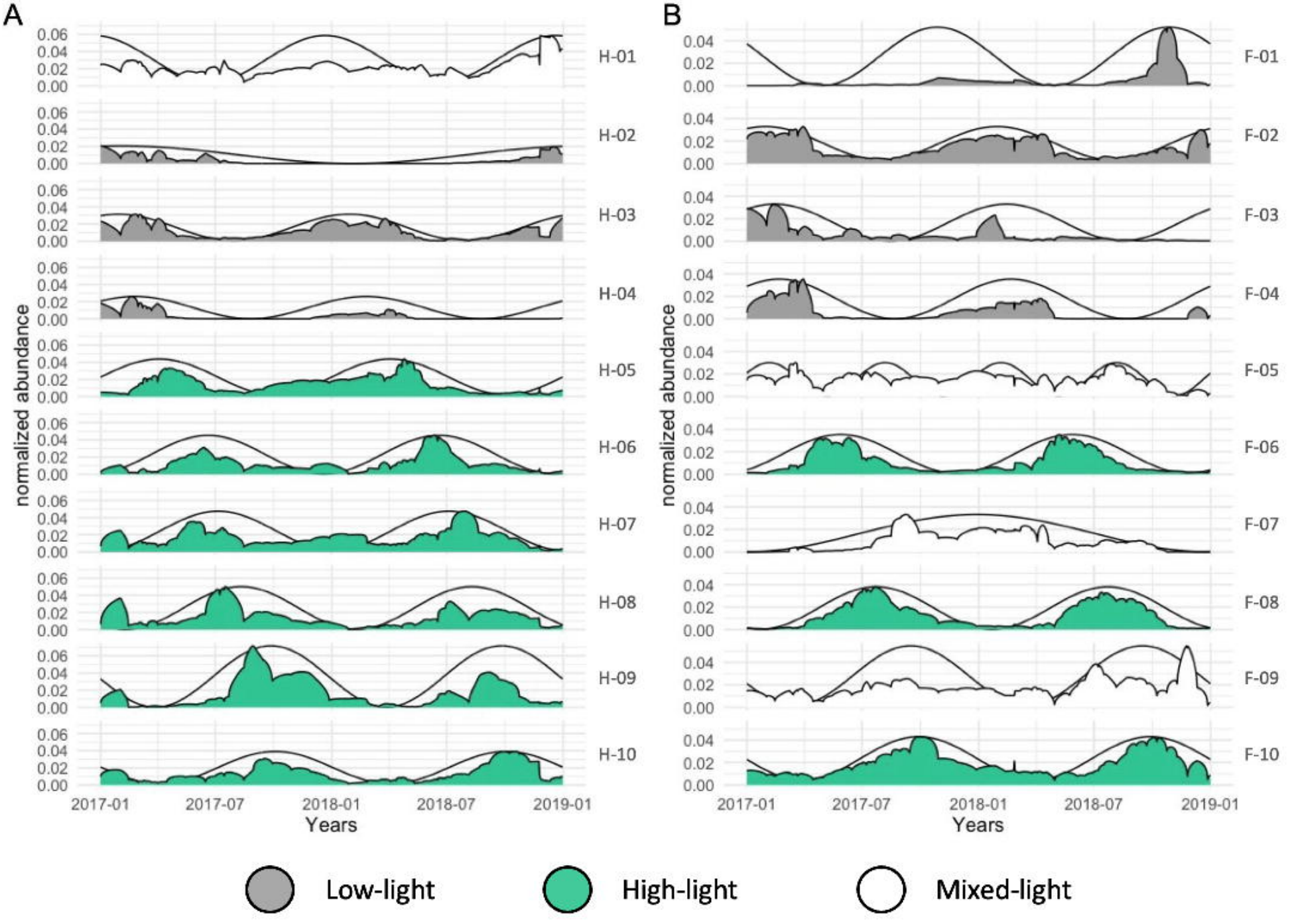
A
B
H-01
H-02
H-03
H-04
H-05
H-06
H-07
H-08
H-09
H-10
F-01
F-02
F-03
F-04
F-05
F-06
F-07
F-08
F-09
F-10
normalized abundance
0.06
0.04
0.02
0.00
2017-01
2017-07
2018-01
2018-07
2019-01
Years
Low-light
High-light
Mixed-light

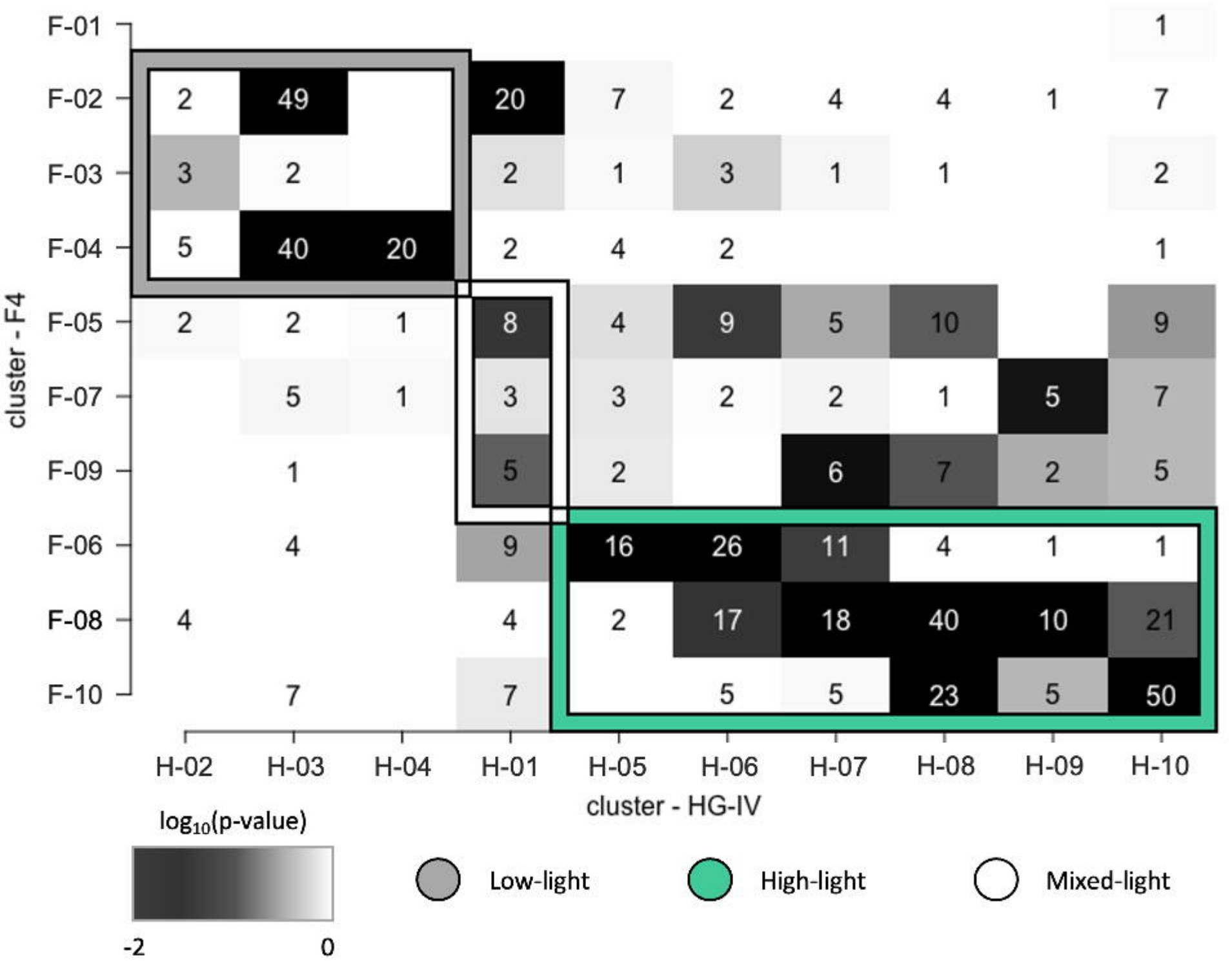
F-01
F-02
F-03
F-04
F-05
F-07
F-09
F-06
F-08
F-10
cluster - F4
H-02
H-03
H-04
H-01
H-05
H-06
H-07
H-08
H-09
H-10
cluster - HG-IV
log10(p-value)
-2
0
Low-light
High-light
Mixed-light

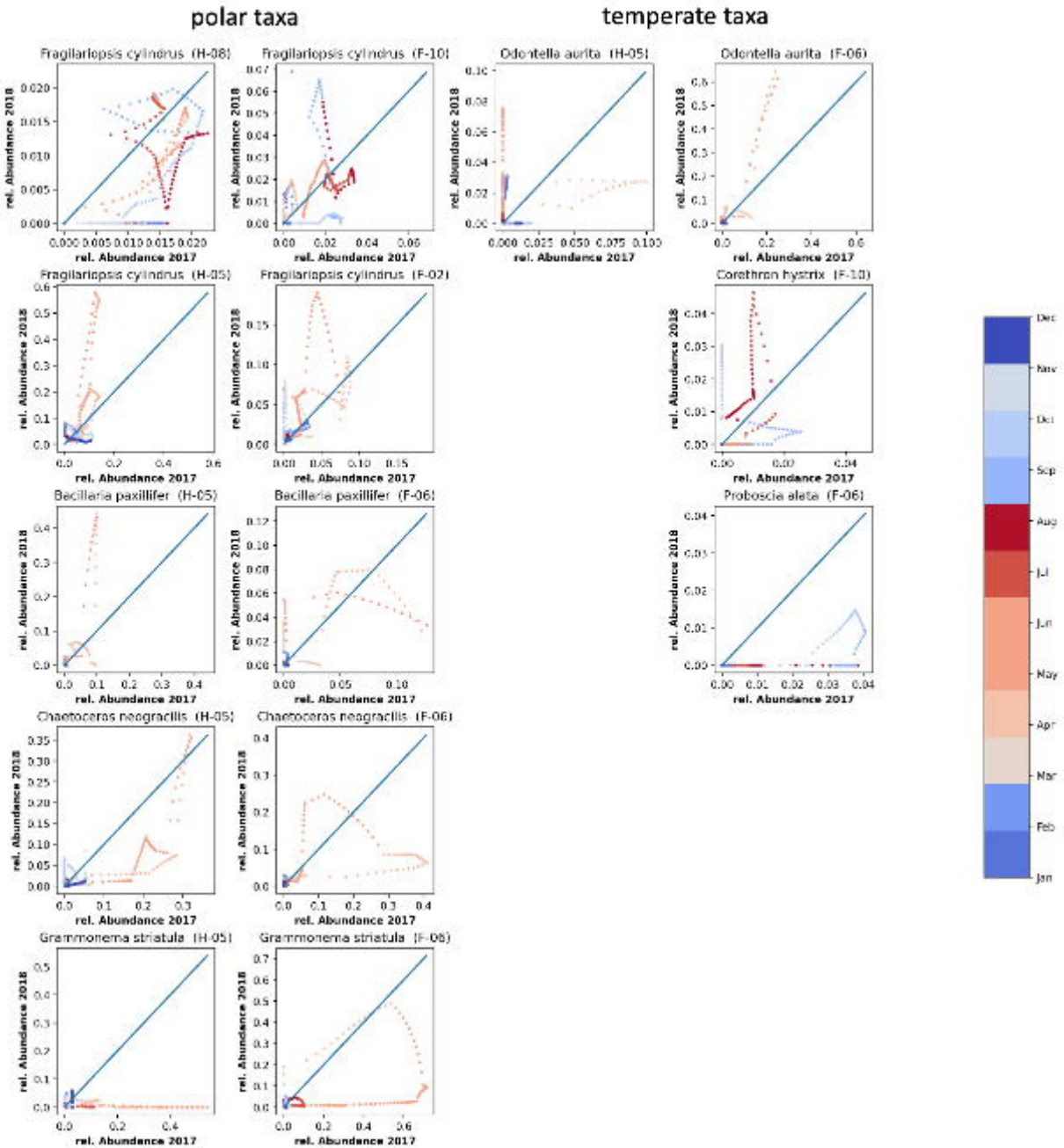
polar taxa
temperate taxa
Fragilariopsis cylindrus (H-08)
Fragilariopsis cylindrus (F-10)
Odontella aurita (H-05)
Odontella aurita (F-06)
Fragilariopsis cylindrus (H-05)
Fragilariopsis cylindrus (F-02)
Corethron hystrix (F-10)
Bacillaria paxillifer (H-05)
Bacillaria paxillifer (F-06)
Proboscia alata (F-06)
Chaetoceros neogracilis (H-05)
Chaetoceros neogracilis (F-06)
Grammonema striatula (H-05)
Grammonema striatula (F-06)
rel. Abundance 2018
rel. Abundance 2017
Dec
Nov
Oct
Sep
Aug
Jul
Jun
May
Apr
Mar
Feb
Jan

$$s(t) = \frac{f_2(t)}{f_0(t)}, \tag{1}$$

$$p(x,y) = \frac{\mathrm{MWR}|_x}{\mathrm{MWR}|_y}, \qquad x \in X, y \in Y, \tag{2}$$

$$t(x,y) = \frac{\mathrm{MLR}|_x}{\mathrm{MLR}|_y}, \qquad x \in X, y \in Y, \tag{3}$$

$$q(z) = \frac{\frac{1}{|\mathrm{MWR}|_z|} \sum_{i \in \mathrm{MWR}|_z} {}_i\mathrm{MWR}|_z}{\frac{1}{|\mathrm{MLR}|_z|} \sum_{h \in \mathrm{MLR}|_z} {}_h\mathrm{MLR}|_z}, \qquad z \in Z, \tag{4}$$

Table 1: **Cluster Overview with the ten clusters for the moorings F4 and HG-IV:** The cluster names, light types (high-light (HL), low-light (LL), mixed-light (NA)), the number of peaks and the total cluster size of ASV and the percent size, the s-score that measures the seasonality, the area under the curve (AUC) for both years (see methods), the quotients of those years and the number of ASV that only occur on this mooring: absolute (MS(abs)) and relative values (in %) (MS(rel)) (MS: mooring specific).

name	type	#peaks	cl_size	cl_size %	s-score	AUC17	AUC18	AUC17/18	AUC18/17	MS(abs)	MS(rel)
H-01	NA	2	72	9	0.18	6.9837	8.8812	0.7863	1.2717	12	16.67
H-02	LL	1	68	8	0.39	1.81	1.0084	1.7949	0.5571	52	76.47
H-03	LL	2	151	18	0.44	4.4387	4.1164	1.0783	0.9274	41	27.15
H-04	LL	2	50	6	0.83	1.7481	0.7188	2.432	0.4112	28	56
H-05	HL	2	76	9	0.33	5.2585	5.1262	1.0258	0.9748	37	48.68
H-06	HL	2	87	10	0.41	4.1827	4.7476	0.881	1.1351	21	24.14
H-07	HL	2	65	8	0.2	6.0155	6.5539	0.9179	1.0895	13	20
H-08	HL	2	113	14	0.32	6.6398	4.405	1.5073	0.6634	23	20.35
H-09	HL	2	33	4	0.53	7.9501	4.5641	1.7419	0.5741	9	27.27
H-10	HL	2	122	15	0.41	5.0174	5.0116	1.0012	0.9988	18	14.75
F-01	LL	2	27	3	0.66	0.6775	2.8243	0.2399	4.1687	26	96.3
F-02	LL	2	144	16	0.39	5.4081	5.1656	1.0469	0.9552	48	33.33
F-03	LL	2	33	4	0.46	3.289	1.228	2.6783	0.3734	18	54.55
F-04	LL	2	168	19	0.75	2.9621	1.8344	1.6148	0.6193	94	55.95
F-05	NA	1	61	7	0.06	6.194	5.2571	1.1782	0.8487	11	18.03
F-06	HL	2	109	12	0.58	3.9653	4.1903	0.9463	1.0567	37	33.94
F-07	NA	4	53	6	0.13	3.4143	3.529	0.9675	1.0336	24	45.28
F-08	HL	2	142	16	0.58	4.8684	4.4017	1.106	0.9041	26	18.31
F-09	NA	2	36	4	0.17	5.6129	7.6206	0.7365	1.3577	8	22.22
F-10	HL	2	130	12	0.34	7.0415	7.0604	0.9973	1.0027	28	21.54